J|A|C|S
ARTICLES
Published on Web 10/15/2005

# Raman and IR Spectroscopy of Chemically Processed Single-Walled Carbon Nanotubes

Un Jeong Kim,[†] Clascidia A. Furtado,[‡] Xiaoming Liu,[†] Gugang Chen,[†] and Peter C. Eklund*,[†,§]

*Contribution from the Departments of Physics and Materials Science, The Pennsylvania State University, University Park, Pennsylvania 16802, and Centro de Desenvolvimento da Tecnologia Nuclear, CDTN/CNEN, Belo Horizonte, MG, Brazil*

Received May 5, 2005; E-mail: pce3@psu.edu

***Abstract:*** IR and Raman spectroscopy has been used to study the evolution of the vibrational spectrum of bundled single-walled carbon nanotubes (SWNTs) during the purification process needed to remove metal catalyst and amorphous carbon present in arc-derived SWNT soot. We have carried out a systematic study to define the different outcomes stemming from the purification protocol (e.g., DO, DO/HCl, DO/$HNO_3$, $H_2O_2$, $H_2O_2$/HCl), where dry oxidation (DO) or refluxing in $H_2O_2$ was used in a first purification step to remove amorphous carbon. The second step involves acid reflux (HCl or $HNO_3$) to remove the residual growth catalyst (Ni−Y). During strong chemical processing, it appears possible to create additional defects where carbon atoms are eliminated, the ring structure is now open, localized C=C bonds are created, and O-containing groups can be added to this defect to stabilize the structure. Evolution of SWNT skeletal disorder obtained via chemical processing was studied by Raman scattering. Higher intensity ratios of R- and G-band ($I_R/I_G$) are more typically found in SWNT materials with low D-band intensity and narrow G-band components. Using IR transmission through thin films of nanotubes, we can resolve the structure due to functional groups that were present in the starting material or added through chemical processing. After high-temperature vacuum annealing of the purified material at 1100 °C, IR spectroscopy shows that most of the added functional groups can be removed and that the structure that remains is assigned to the one- and two-phonon modes of SWNTs.

Downloaded via AGH UNIV OF SCIENCE AND TECHNOLOGY on January 11, 2022 at 09:11:59 (UTC).
See https://pubs.acs.org/sharingguidelines for options on how to legitimately share published articles.

## Introduction

Single-walled carbon nanotubes present many exciting opportunities for fundamental science and new technologies.[1] An unfortunate outcome of many growth processes that produce large batches of bundled, free-standing single-walled carbon nanotubes (SWNTs) is that the product is not pure and contains residual growth catalyst and amorphous carbon as important impurities.[2−6] Furthermore, the manufacturing and postsynthesis chemical purification can remove C-atoms from the tube wall and add functional groups to the SWNT surface.

Raman scattering has been used for many years as a probe of disorder in the carbon skeleton of $sp^2$ and $sp^3$ carbon materials.[7] Raman scattering in SWNTs is a diameter-selective resonant scattering process.[8] The scattering is so intense that individual tubes can be studied.[9] Disorder in the tube wall has also been studied by Raman scattering.[10] Similar to studies in other $sp^2$ carbons (including graphite), disorder in the graphene structure of the tube wall leads to the appearance of a broad disorder band or D-band.[11] Recently, this band has been shown to be dispersive (i.e., the position changes with the excitation frequency).[10] Many factors should affect the strength of the

[†] Department of Physics, Penn State University.
[‡] Centro de Desenvolvimento da Tecnologia Nuclear.
[§] Department of Materials Science, Penn State University.

(1) (a) Rinzler, A. G.; Hafner, J. H.; Nikolaev, P.; Lou, L.; Kim, S. G.; Tomanek, D.; Colbert, D.; Smalley, R. E. *Science* **1995**, *269*, 1550. (b) Wang, Q. H.; Setlur, A. A.; Lauerhaas, J. M.; Dai, J. Y.; Seelig, E. W.; Chang, R. H. *Appl. Phys. Lett.* **1998**, *72*, 2912. (c) Choi, W. B.; Chung, D. S.; Kang, J. H.; Kim, H. Y.; Jin, Y. W.; Han, I. T.; Lee, Y. H.; Jung, J. E.; Lee, N. S.; Park, G. S.; Kim, J. M. *Appl. Phys. Lett.* **1999**, *75*, 20. (d) Kim, W.; Choi, H. C.; Shim, M.; Li, Y. M.; Wang, D. W.; Dai, H. J. *Nano Lett.* **2002**, *2* (7), 703.
(2) Rinzler, A. G.; Liu, J.; Dai, H.; Nikolaev, P.; Huffman, C. B.; Rodriguez-Macias, F. J.; Boul, P. J.; Lu, A. H.; Heymann, D.; Colbert, D. T.; Lee, R. S.; Fischer, J. E.; Rao, A. M.; Eklund, P. C.; Smalley, R. E. *Appl. Phys. A* **1998**, *67* (1), 29.
(3) Chiang, I. W.; Brinson, B. E.; Huang, A. Y.; Willis, P. A.; Bronikowski, M. J.; Margrave, J. L.; Smalley, R. E.; Hauge, R. H. *J. Phys. Chem. B* **2001**, *105* (35), 8297.
(4) Harutyunyan, A. R.; Pradhan, B. K.; Chang, J. P.; Chen, G.; Eklund, P. C. *J. Phys. Chem. B* **2002**, *106*, 8671.
(5) Furtado, C. A.; Kim, U. J.; Gutierrez, H. R.; Pan, L.; Dickey, E. C.; Eklund, P. C. J. *Am. Chem. Soc.* **2004**, *126*(19), 6095.
(6) Zhou, O.; Gao, B.; Bower, C.; Fleming, L.; Shimoda, H. *Mol. Cryst. Liq. Cryst. Sci. Technol., Sect. A* **2000**, *340*, 541.
(7) *Analytical Applications of Raman Spectroscopy*; Michael J. Pelletier, Ed.; Blackwell Science: Cambridge, MA, 1999.
(8) Rao, A. M.; Richter, E.; Bandow, S.; Chase, B.; Eklund, P. C.; Williams, K. A.; Fang, S.; Subbaswamy, K. R.; Menon, M.; Thess, A.; Smalley, R. E.; Dresselhaus, G.; Dresselhaus, M. S. *Science* **1997**, *275*, 187.
(9) (a) Jorio, A.; Saito, R.; Hafner, J. H.; Lieber, C. M.; Hunter, M.; McClure, T.; Dresselhaus, G.; Dresselhaus, M. S. *Phys. Rev. Lett.* **2001**, *86* (6), 1118. (b) Dresselhaus, M. S.; Dresselhaus, G.; Jorio, A.; Souza, A. G.; Saito, R. *Carbon* **2002**, *40* (12), 2043.
(10) (a) Pimenta, M. A.; Jorio, A.; Brown, S. D. M.; Filho, A. G. S.; Dresselhaus, G.; Hafner, J. H.; Lieber, C. M.; Saito, R.; Dresselhaus, M. S.; Endo, M. *Phys. Rev. B* **1999**, *59*, R6585. (b) Matthews, M. J.; Pimenta, M. A.; Dresselhaus, G.; Dresselhaus, M. S.; Endo, M. *Phys. Rev. B* **2000**, *64*, R041401.
(11) (a)Wang, Y.; Alsmeyer, D. C.; McCreery, R. L. *Chem. Mater.* **1990**, *2*, 557. (b) Tunistra, F.; Koenig, J. L. *Chem. Phys.* **1970**, *53*, 1126. (c) Eklund, P. C.; Holden, J. M.; Jishi, R. A. *Carbon* **1995**, *33*, 959.

D-band scattering (any change in the C-atom environment that affects the periodicity of the carbon structure (e.g., missing C-atoms and functional groups that are either added intentionally[12,13] or added unintentionally during growth or in post growth purification)[4−6,14−16]). Raman scattering, although a powerful probe of the nanotube phonons and optical excitations, has not been able to detect the identity of functional groups present on the tube walls. Raman scattering, therefore, has not been found very helpful in studying the chemistry of the nanotube wall.

Infrared (IR) spectroscopy, on the other hand, has shown significant promise for the study of SWNT wall chemistry.[12−21] Several examples of tube wall functionalization have been reported where IR spectra were used to identify the functional groups added to the tube wall (e.g., −COOH, −OH, other oxygen containing groups,[12,13,16−18] C−F,[15] -R-oxycarbonyl nitrenes,[19] C−$Cl_2$,[20] and −CH).[21]

Here, we investigate several postsynthesis SWNT purification protocols that are found popular in the literature. There are three sequential steps in the SWNT purification process: (1) oxidation to remove amorphous carbon; (2) acid reaction to remove the metal growth catalyst (sometimes the metal surface is passivated by a shell of carbon); (3) and high-temperature annealing to remove functional groups that may have been added to the tube wall in the acid reaction and oxidation steps.[5,13]

Two of the most common methods for the removal of amorphous carbon (AC) attempt to take advantage of the higher reactivity of AC with oxygen relative to SWNTs. In one case, a dry oxidation in air at elevated temperatures is carried out.[2,4,5] Success has also been reported using hydrogen peroxide $H_2O_2$.[6] We consider the changes to the tube wall for both of these approaches. The second step of purification involves the removal of the metal with acids: usually $HNO_3$[5] or HCl[4,5] is used. $HNO_3$ has been reported, in extreme chemical conditions, to aggressively attack the tube walls, while HCl is found to be passive with respect to attack on the carbons in the sample. If the metal catalyst in the nanotube soot is covered with a graphitic shell of carbon, the oxidation step is also important to weaken this coating for subsequent acid digestion of the metal. It is also important to neutralize the sample after the acid step.[5] The third step, high temperature annealing, is carried out either in a vacuum or in flowing inert gas and usually in the range of ∼800−1100 °C.

In this paper, we investigate with Raman and IR spectroscopy how the various protocols outlined here affect the carbon skeleton and the attachment of functional groups. Although there has been considerable work invested to learn how to purify SWNT material, to the best of our knowledge, nobody has used both IR and Raman spectroscopy together to follow the evolution of the SWNT material through these purification steps.

## Experimental Procedures

Arc discharge nanotube soot was obtained from Carbolex, Inc. The tubes were produced using ∼4 atomic % Ni−Y loaded carbon electrodes. One large batch from the vendor was homogenized and studied here. The as-delivered material was found to contain bundles of ∼100−400 SWNTs, ∼1−5 $\mu$m long, and with mean nanotube diameter ∼1.4 nm, with most of the nanotubes in the diameter range of 1.2−1.6 nm, as determined by cross-sectional views of the bundle imaged by HRTEM.[22] Also present in the soot is ∼20−30 wt % amorphous carbon and ∼30 wt % of ∼20 nm diameter carbon-coated Ni−Y particles, as determined by thermogravimetric analysis in air, [TGA; (TA Instruments, model SDT 2960)].[4]

To optimize the dry oxidation (DO) step, TGA was carried out first. It was determined that a thermal soak at 355 °C for 20 min in flowing dry air (100 sccm) was required to achieve selective oxidation of the amorphous carbon, while minimizing nanotube mass loss. Wet oxidation removal of AC was carried out by refluxing in 30 vol % of $H_2O_2$ in $H_2O$ for 6 h. The solution was then filtered through a ∼1 $\mu$m pore-size polycarbonate membrane (Whatman, Inc.). It was found necessary to repeat this procedure ($H_2O_2$ reflux/filter/wash process) 3 times to remove most of the AC.

For metal removal (Ni−Y), we refluxed the material produced by step 1 either in a strongly oxidizing 3 N $HNO_3$ solution for 16 h or in a weakly oxidizing 6 N HCl solution for 24 h. The details of metal removal procedure can also be found in ref 5. Using TGA to analyze the product after these two steps in the purification process, the wt % of nanotubes in the sample increased to approximately 90% ($HNO_3$) or 85% (HCl), independent of whether a wet ($H_2O_2$) or dry (air) oxidation was carried out. The remainder of the solids at this stage of purification typically was ∼8−12 wt % AC and ∼1−2 wt % metal. The details of how to interpret the TGA data can be found in ref 4. In the third and final step, we performed a high-temperature vacuum anneal (HTVA) at 1100 °C for 1 h at ∼$10^{-6}$ Torr with a turbo-pumped vacuum system pumping on the sample kept in a open boat in a 1 in. diameter quartz tube centered in a furnace.

FTIR and Raman spectra were both collected using a BOMEM DA3+ FT spectrometer, equipped to do conventional FTIR spectroscopy, or FT-Raman spectroscopy with a Nd:YAG laser (1064 nm). The nanotube material was first ultrasonicated in 2-propanol using a low power bath (Aquasonic, Inc.; Model P250HT). Several drops of the solution were then deposited from solution onto ZnSe substrates maintained in air at ∼60 °C. The solvent from each drop was allowed to evaporate before the next drop was added. In this way, a film of nanotubes was built up such that the transmission of the film was ∼60% at ∼2000 $cm^{-1}$. This transmission value includes the reflection/adsorption losses due to the substrate. The IR spectrum of just the nanotube film was obtained by removing the reflection/adsorption losses from the ZnSe substrate. This normalization was done by measuring the single beam transmission of a clean portion on the substrate and when the beam passed through the SWNT film and substrate; the normalized spectrum is just the ratio of these two spectra. For the IR measurements, the spectral resolution was 4 $cm^{-1}$; for Raman spectroscopy, it was ∼1 $cm^{-1}$.

## Results and Discussion

We first present the results obtained from Raman scattering that focus on the evolution of SWNT skeletal disorder obtained via chemical processing and repaired through HTVA. The

(12) Kukovecz, A.; Kramberger, C.; Holzinger, M.; Kuzmany, H.; Schalko, J.; Mannsberger, M.; Hirsch, A. *J. Phys. Chem. B* **2002**, *106* (25), 6374.
(13) Martinez, M. T.; Callejas, M. A.; Benito, A. M.; Cochet, M.; Seeger, T.; Anson, A.; Schreiber, J.; Grodon, C.; Marhic, C.; Chauvet, O.; Fierro, J. L. G.; Maser, W. K. *Carbon* **2003**, *41*, 2247.
(14) Pehrsson, P. E.; Zhao, W.; Baldwin, J. W.; Song, C. H.; Liu, J.; Kooi, S.; Zheng, B. *J. Phys. Chem. B* **2003**, *107* (24), 5690.
(15) (a) Stevens, J. L.; Huang, A. Y.; Peng, H. Q.; Chiang, L. W.; Khabashesku, V. N.; Margrave, J. L. *Nano Lett.* **2003**, *3* (3), 331. (b) Gu, Z.; Peng, H.; Hauge, R. H.; Smalley, R. E.; Margrave, J. L. *Nano Lett.* **2002**, *2* (9), 1009.
(16) Zhang, J.; Zou, H.; Qing, Q.; Yang, Y.; Li, Q. Q.; Liu, Z.; Gao, X.; Du, Z. *J. Phys. Chem. B* **2003**, *107* (16), 3712.
(17) Hamon, M. A.; Bhowmik, H.; Hu, P.; Niyogi, S.; Zhao, B.; Itkis, M. E.; Haddon, R. C. *Chem. Phys. Lett*. **2001**, *347*, 8.
(18) Mawhinney, D. B.; Naumenko, V.; Kuznetsova, A.; Yates, J. T.; Liu, J.; Smalley, R. E. *J. Am. Chem. Soc.* **2000**, *122* (10), 2383.
(19) Holzinger, M.; Abraha, J.; Whelan, P.; Graupner, R.; Ley, L.; Hennrich, F.; Kappes, M.; Hirsch, A. *J. Am. Chem. Soc.* **2003**, *125* (28), 8566.
(20) Hu, H.; Zhao, B.; Hamon, M. A.; Kamaras, K.; Itkis, M. E.; Haddon, R. C. *J. Am. Chem. Soc.* **2003**, *125* (48), 14893.
(21) Khare, B. N.; Meyyappan, M.; Cassell, A. M.; Nguyen, C. V.; Han, J. *Nano Lett*. **2002**, *2* (1), 73.
(22) Kim, U. J.; Gutierrez, H. R.; Crespi, V. H.; Kim, J. P.; Eklund, P. C. manuscript in preparation.

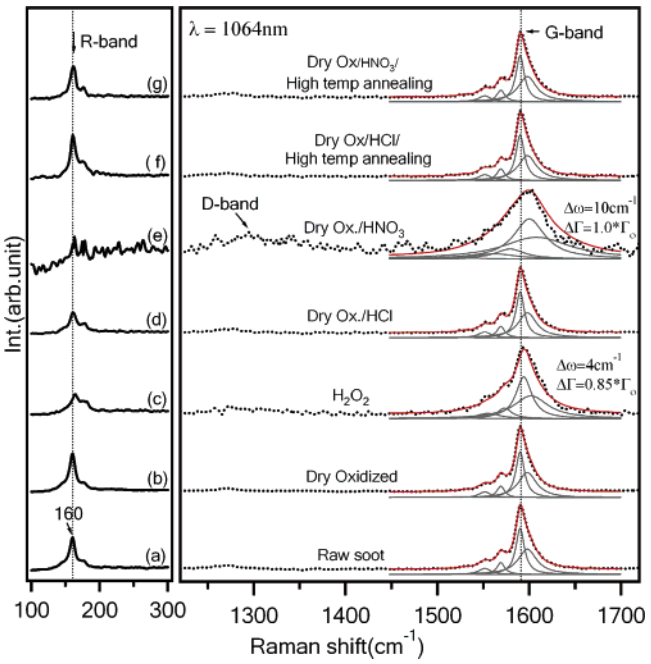


***Figure 1.*** Raman spectra of various SWNT films: R-band (100−300 $cm^{-1}$) region (left panel) and D- and G-band (1230−1750 $cm^{-1}$) (right panel). From bottom to top, the spectra refer to raw soot (a), DO at 355 °C for 20 min (b), $H_2O_2$ reflux (c), DO/HCl (d), DO/$HNO_3$ (e), DO/HCl/HTVA at 1100 °C (f), and DO/$HNO_3$/HTVA at 1100 °C (g). All spectra were normalized to yield the same intensity for the band at ∼1590 $cm^{-1}$. For the definitions of these processing labels, please see the text. The values $\Delta\omega$ and $\Delta\Gamma$ in the figure indicate the rigid shift of all G-components and the universal increase in their full width at half-maximum (fwhm) $\Delta\Gamma$, respectively. $\Gamma_o$ is the fwhm of the raw soot.

scattering was excited using 1064 nm Nd:YAG radiation, which is known to couple to semiconducting nanotubes in our samples that have diameters in the range of 1.2−1.6 nm.[23] These semiconducting tubes are easier to study because the Raman modes are not broadened by interaction with the free carriers as they are in metallic tubes. In this case, the Raman lines can take on a decidedly broader Breit−Wigner−Fano line profile.[24] The first-order allowed Raman lines for semiconducting SWNTs should have a Lorentzian profile.

Figure 1 shows the Raman spectra of SWNT materials from the raw soot and processed by various protocols as discussed previously. The spectra appear in two panels: 100−300 and 1230−1750 $cm^{-1}$. The intensity of all the spectra in Figure 1 were normalized to yield the same intensity for the G-band at ∼1590 $cm^{-1}$. The Raman spectra, from bottom to top in the figure, refer to raw soot (a), raw soot after DO at 355 °C for 20 min (b), raw soot after $H_2O_2$ reflux (c), raw soot after DO/HCl (d), and then the sequences DO/$HNO_3$ (e), DO/HCl/HTVA at 1100 °C (f), and DO/$HNO_3$/HTVA at 1100 °C (g).

The Raman-active radial breathing modes (R-band) are observed at low frequency in the left-hand panel of Figure 1. The R-band can have contributions from several tubes simultaneously in resonance with the laser photon frequency. Each component in the R-band has a frequency approximately given by $\omega_{RBM} = 223.7\ cm^{-1}(nm)/d_t(nm)$,[8] where $d_t$ is the tube diameter. This relation is approximate in that it neglects a small (calculated) restoring force that adds 12−14 $cm^{-1}$ to the $1/d$ term. For more information on this detail, the readers are referred to ref 25. It is clear from the R-band that at least two distinct radii tubes exist in the CarboLex material when excited with 1064 nm radiation (i.e., $d \sim 1.24$ and 1.40 nm). In the 1230−1750 $cm^{-1}$ region (right-hand panel), two Raman bands are observed: a relatively broad band near ∼1300 $cm^{-1}$ and a stronger band with structure in the ∼1580−1600 $cm^{-1}$ region. The band with maximum near ∼1300 $cm^{-1}$ is common in disordered $sp^2$ carbon material and has been called the D-band. It is activated by disorder in the $sp^2$ carbon network. The band at ∼1590 $cm^{-1}$ is close to that observed for well-ordered graphite (i.e., $E_{2g}$ band at 1582 $cm^{-1}$), and it is therefore often called the G-band. The G-band in well-ordered nanotubes actually has several components that stem from the perfect cylindrical symmetry of the nanotube. The D-band intensity, and G-bandwidth, have both been considered as probes of SWNT wall integrity or functionalization on the tube walls.[5,7]

We have fit the G-bands in Figure 1 to a sum of four Lorentzian components. The components can be broadened by disorder in the SWNT skeletal structure. To take advantage of this link between Raman line width and order in the carbon skeleton of the SWNT, we have had to carry out a careful line shape analysis. The solid line in the figure is the result of our line shape analysis. We find that the Lorentzian line width parameters for the G-band components of the raw soot are not affected by either dry oxidation (DO) or by a two-step treatment involving dry oxidation followed by HCl treatment (DO/HCl). This suggests that these chemical processing steps produce little or no change in the carbon skeleton of the SWNT. Similarly, there is no increase in intensity in the D-band after DO or DO/HCl processing. However, this is not the case for wet oxidation ($H_2O_2$) to remove amorphous carbon or after using 3 N $HNO_3$ to digest metallic particles. In the case of this chemical processing, very noticeable changes in the Raman spectrum can be observed, even by examining the Raman spectra by eye (Figure 1). For $H_2O_2$ processing only (Figure 1c) and DO/$HNO_3$ processing (Figure 1e), a careful line shape analysis was also carried out. After this chemical processing, the G-band could be well-fitted by a simple rigid upshift of the four Lorentzian components identified in the spectrum of the raw soot (i.e., all relative intensities of the G-band components remain the same, but all the components were broadened by the same amount). The results of these G-band analyses are seen as the solid curves passing through the data in Figure 1. After $H_2O_2$ reflux, and also after DO/$HNO_3$ processing, we find that the G-band components are broadened by factors of 1.8 and 2, respectively. Furthermore, the G-band has upshifted by ∼4 $cm^{-1}$ ($H_2O_2$) and ∼10 $cm^{-1}$ ($HNO_3$). Previous experimental and theoretical work has shown that doping SWNTs with either electron donors or acceptors[26,27] results in noticeable shifts in the high-frequency vibrational modes. Removing electrons from SWNT (i.e.,

(23) Kataura, H.; Kumazawa, Y.; Maniwa, Y.; Umezu, I.; Suzuki, S.; Ohtsuka, Y.; Achiba, Y. *Synth. Met.* **1999**, *103*, 2555.
(24) Pimenta, M. A.; Marucci, A.; Empedocles, S. A.; Bawendi, M. G.; Hanlon, E. B.; Rao, A. M.; Eklund, P. C.; Smalley, R. E.; Dresselhaus, G.; Dresselhaus, M. S. *Phys. Rev. B* **1998**, *58*, 16016.
(25) (a) Kim, U. J.; Gutierrez, H. R.; Kim, J. P.; Eklund, P. C. *J. Phys. Chem. B*, in press. (b) Gutierrez, H. R.; Kim, U. J.; Kim, J. P.; Eklund, P. C. *Nano Lett.*, in press. (c) Alvarez, L.; Righi, A.; Guillard, T.; Rols, S.; Anglaret, E.; Laplaze, D.; Sauvajol, J. *Chem. Phys. Lett.* **2000**, *316*, 186.
(26) (a) Rao, A. M.; Eklund, P. C.; Bandow, S.; Thess, A.; Smalley, R. E. *Nature* **1997**, *388*, 257. (b) Chen, G.; Bandow, S.; Margine, E. R.; Nisoli, C.; Kolmogorov, A. N.; Crespi, V. H.; Gupta, R.; Sumanasekera, G. U.; Iijima, S.; Eklund, P. C. *Phys. Rev. Lett.* **2003**, *90* (25), 257403. (c) Chen, G.; Furtado, C. A.; Bandow, S.; Eklund, P. C. *Phys. Rev. B* **2005**, *75* (4).
(27) Sumanasekera, G. U.; Allen, J. L.; Fang, S. L.; Loper, A. L.; Rao, A. M.; Eklund, P. C. *J. Phys. Chem. B* **1999**, *103* (21), 4292.

p-doping or oxidizing) has been shown to result in an upshift in the G-band peak,[25,26] as observed here. This conclusion is consistent with extensive observations of chemical charge-transfer reactions in graphite,[28a] $C_{60}$,[28b] and in SWNTs.[26,27] An upshift of the G-band after refluxing SWNT samples in $HNO_3$ has been observed by several groups.[5,6,12] They identified the upshift of the G-band with electron transfer from the nanotube bundle to form $NO_3^-$ anions. This interpretation is consistent with work in graphite intercalation compounds.[27] For the case of $H_2O_2$, the identity of the anion formed as a result of the refluxing is less clear. In fact, the G-band upshift in this case is probably associated with negative −OH groups chemically bonded to the tube walls. This proposal is consistent with our IR results, which we discuss further next.

The intensity of the D-band in SWNT soot processed by DO/$HNO_3$ or just by $H_2O_2$ is enhanced. The band also broadens and upshifts. The upshift of the D-band is large (∼30 $cm^{-1}$) for DO/$HNO_3$. It should be noted that the D-band is a dispersive Raman band whose position changes with the excitation laser frequency.[10] It is not unexpected that the D-band should also shift at the same time the G-band is upshifting; this is just another signal of charge transfer. Of course, the increase in the D-band intensity should be interpreted as a decrease in the structural order in the SWNT bundles. It is likely that the disorder stems from three factors: added functional groups, missing carbon atoms in the wall, and inhomogeneous decoration of the tube wall by $NO_3^-$ anions. It is well-known that introducing disorder to an $sp^2$ carbon network introduces a broad disorder-induced D- band at ∼1350 $cm^{-1}$. It is less well-known that a second disorder-induced band often appears as a high frequency shoulder to the G-band. This shoulder is located at ∼1620 $cm^{-1}$ and is referred to as the G*-band.[7] In the current study, although we cannot see direct evidence for this G*-band as a shoulder to the G-band, we do observe an increase in scattering intensity on the high-frequency side of the G-band. It was found necessary to incorporate a broad Lorentzian band centered near ∼1600 $cm^{-1}$ to fit Raman spectra to account for this scattering. It could well be that the presence of this 1600 $cm^{-1}$ component in our fits is just a measure of new G* scattering.

We also considered the processing combination of $H_2O_2$/HCl for the first two steps. However, we have not shown the Raman spectrum of $H_2O_2$/HCl in Figure 1 since the subsequent HCl step has no measurable effect on the Raman spectrum.

Finally, it is very interesting to observe the changes in the Raman spectrum associated with HTVA (high-temperature vacuum annealing). As observed in the Raman spectrum of Figure 1f,g, a vacuum anneal at 1100 °C for 1 h on DO/HCl and DO/$HNO_3$ processed material is very dramatic. All the lines narrow, the D-band intensity decreases, and the Raman spectrum returns to that of the raw soot. This indicates that most of the wall disorder introduced by chemical processing can be removed by the HTVA step. In fact, it appears that the skeletal holes (i.e., missing C-atoms) produced in the SWNT wall may drift to the open tube ends where they evaporate. We can observe the removal of the functional groups via IR spectroscopy, as discussed next.

Although the physical or chemical reasons are not yet clear, we find that the ratio of the scattering intensity in the R-band ($I_R$) to that of the G-band ($I_G$) is sensitive to the chemical processing. Our results show that higher ratios of $I_R/I_G$ are more typically found in SWNT materials with low D-band intensity and narrow G-band components. In the case of DO/HCl processing, it is difficult to notice any significant change in either the D-band intensity or the G-band component width relative to that in the raw soot. However, the ratio $I_R/I_G$ changes noticeably. After HTVA, the $I_R/I_G$ ratio increases, and the ratio returns to that observed in the raw soot. We propose that the decrease in $I_R/I_G$ is associated with a reduction in $I_R$. $I_R$ is therefore proposed to be more sensitive to disorder than $I_G$.

The major impact of chemical treatment on the R-band is a reduction of intensity. However, we can also say the following about the effects of chemical treatment on the R-band frequency: (1) HCl has little or no effect on the R-band frequency; (2) $H_2O_2$ produces a small upshift of ∼4 $cm^{-1}$; and (3) $HNO_3$ may produce a small (∼1−2 $cm^{-1}$) upshift, but this upshit is difficult to quantify given the weak nature of the R-band after nitric acid treatment. It is interesting to consider why the shift of the G- and D-band can be so easily observed while the R-band shift is so small as to be difficult to measure. The reasons could be many (e.g., the difference in the percent effects of doping on the bond bending vs bond stretching force constants and the admixture of the bond bending and stretching in the various eigenmodes (e.g., R-, D-, and G-) are different and therefore a complicating factor). However, consider the following argument. If we say that the mode frequency is simply related to the square root of the change in an effective force constant, then a 0.1% change in the effective force constant for a particular mode leads to a 0.05% change in the mode frequency. Further, if we consider the same percent change in the effective force constant for the modes at ∼160 $cm^{-1}$ (R), ∼1300 $cm^{-1}$ (D), and ∼1600 $cm^{-1}$ (G), then we would expect the same percentage shift in the R-, D-, and G-mode frequencies. However, in terms of the actual $cm^{-1}$ shift, the high frequency modes would then upshift much more than the R-bands because they have significantly higher frequency (i.e., a 10 $cm^{-1}$ upshift of the G-band is equivalent to a ∼1 $cm^{-1}$ upshift in a ∼160 $cm^{-1}$ R-band mode). It is difficult at this time to separate out the effects of strain due to adding functional groups to the tube wall and the effects of strain due to electron transfer to (or from) the carbon skeleton. Compressive strain of the C−C bond or a change of the bond angles can lead to an upshift in vibrational mode frequencies. We can add that studies of charge transfer-induced strain in graphite intercalation compound space (GICs) have found similar upshifts to what we observe in carbon nanotubes exposed to nitric acid or hydrogen peroxide. For example, the reaction of nitric acid with graphite under mild conditions is thought to lead to the intercalation of nitrate ion between the graphene layers, which removes electrons from the $sp^2$ carbon network and induces an upshift in the G-band of the GIC by ∼10−20 $cm^{-1}$, similar to what is observed here for SWNTs. In the case of GICs, it is thought that the reaction with nitric acid under mild conditions does not disrupt the carbon skeleton via the removal of carbon and/or the addition of functional groups.

We have also examined HRTEM images of bundles of SWNTs that were subjected to various chemical processes. Inspection of these images indicates to us that HRTEM is far

(28) (a) Eklund, P. C.; Subbaswamy, K. R. *Phys. Rev. B* **1992**, *20*, 5157−5161. (b) Zhou, P.; Wang, K.-A.; Wang, Y.; Eklund, P. C.; Dresselhaus, M. S.; Dresselhaus, G.; Jishi, R. A. *Phys. Rev. B 46*, 2595.

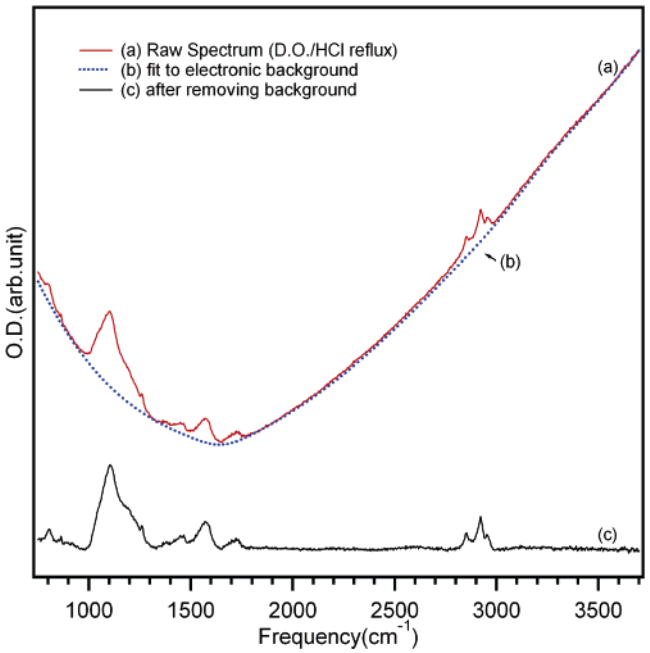


***Figure 2.*** Optical density in the mid-IR for a DO/HCl SWNT sample (a) and a fit (b) to a smooth polynomial background (dotted line). The difference spectrum (a and b) appears at the bottom of the figure. The coefficients of the cubic polynomial are adjusted to yield a flat baseline for the difference spectrum.

less sensitive in exposing disorder in the carbon skeleton than Raman scattering. Only under extreme processing conditions in $HNO_3$ were we able to see evidence of large holes in the nanotube wall. We can conclude that Raman scattering is far better a probe of disorder when the tube walls are largely intact.

Next, we show how the IR spectroscopy of SWNT material during processing can be used as an important complementary probe to Raman scattering. We follow the evolution of the IR spectrum with the same set of samples as discussed previously. Unfortunately, the IR activity associated with added functional groups is somewhat difficult to observe. After chemical processing, the wt % fraction of the sample identified with functional groups is perhaps on the order of ~5 wt %, at the most. Only those groups that are most numerous and those having strong IR activity will be detected. Furthermore, the optical absorption in the mid-IR region is dominated by electronic contributions from the SWNTs. To see the vibrational modes of the functional groups (and the IR modes of SWNT[29]), the electronic contribution should be removed from the spectrum. First, we show how this electronic contribution is removed.

In Figure 2, we show the actual normalized transmission spectrum for a SWNT film on a ZnSe substrate (indicated as spectra a). The effects of reflection/absorption loss in the ZnSe have been removed from spectra a, as discussed in the Experimental Procedures. To enhance the visibility of the sharp structure, we subtract the background identified with the electronic contribution by fitting it to a cubic polynomial, shown as the dotted line spectra b. The difference spectrum (i.e., spectra a and b) is shown at the bottom of Figure 2 as spectra c. The parameters of the cubic polynomial are chosen to produce a flat baseline for spectra c.

(29) Kim, U. J.; Liu, X. M.; Furtado, C. A.; Chen, G.; Saito, R.; Jiang, J.; Dresselhaus, M. S.; Eklund, P. C. *Phys. Rev. Lett.* **2005**, *95*, 157402.

In Figure 3, we show the evolution of the mid-IR spectrum of SWNT material after processing for amorphous carbon removal (i.e., oxidation step). The spectra in Figure 3 are the difference spectra; the particular electronic contribution has been removed. The difference spectrum for the raw soot appears at the bottom, and at the top, we display the difference spectrum of purified material processed by DO/HCl/HTVA = 1100 °C and by DO/$HNO_3$/HTVA = 1100 °C. These top two spectra are for purified and annealed SWNTs. They represent the vibrational contribution of the cleanest material. The structure that appears in these top two spectra should either be identified with SWNT IR modes[29] or with the most tenaciously bound functional groups, or defects. According to studies on other $sp^2$ carbons, on HTVA = 1100 °C, treatment should remove most of the functional groups (the hydrocarbon groups are the most difficult to remove).[30a] These upper two spectra should be very helpful in setting the baseline for intrinsic SWNT IR activity and allow the identification of functional groups that become attached during chemical processing. We begin with a brief description of the structure in these two top spectra. First of all, there are two artifacts identified with the spectrometer in all the spectra in Figure 3: a prominent triplet at 2900 $cm^{-1}$ and a weaker narrow peak at ~1250 $cm^{-1}$.[31] These are identified by the asterisks in the figure. However, the triplet at ~2900 $cm^{-1}$ has been assigned as $C-H_n$ functional groups introduced by atomic hydrogen generated in cold plasma[22] or as a C−H stretching mode of the alkyl chain in octadecylamido (ODA) functionalized SWNTs.[17] In our spectra, we believe that the 2900 $cm^{-1}$ triplet is associated with hydrocarbon contamination in our spectrometer.[31] Most of the peaks in the top two baseline spectra on purified and annealed material in the range of 800−1760 $cm^{-1}$ have been assigned previously to first- and second-order IR modes of SWNTs.[29] It should also be mentioned that all of the structures seen in these top two spectra have also been observed in material vacuum annealed to 1400 °C.[29] So it is unlikely that the peaks in the top two spectra in Figure 3 can be identified with functional groups, as they should be removed during a 1400 °C HTVA.[30a]

We now discuss the new IR bands that appear after chemical processing. For the case of oxidative removal of AC, the results are shown for DO and $H_2O_2$ reflux in the middle of Figure 3. The results after acid processing are shown in Figure 4.

We consider first the IR spectrum of the raw soot (Figure 3a). Many bands from functional groups can be seen in spectrum a that are not present in our baseline spectra Figure 3d,e. For

(30) (a) Kinoshita, K. *Carbon—Electrochemical and Physicochemical Properties*; John Wiley & Sons: New York, 1988; Ch. 3. (b) Pradhan, B. K.; Sandle, N. K. *Carbon* **1999**, *37*, 1323. (c) Fanning, P. E.; Vannice, M. A. *Carbon* **1993**, *31* (5), 721−73.

(31) The identification of a weak structure in the difference spectra of Figures 3 and 4 as due to IR activity of functional group vibrations or long wavelength nanotube phonons requires careful analysis. This difference spectroscopy can pick up spectral artifacts not associated with optical absorption in the sample. The possibility of remnants of spectral structures in the incident photon beam due to the source and optics must therefore be considered. To determine which absorption features in the difference spectrum should be identified with the carbon film, and which should be labeled as artifacts, we carried out optical transmission experiments of a series of samples (same SWNT material) with increasing film thickness. Those peaks identified with true IR absorption in the film grew in intensity with the film thickness and in a correlated way. Two bands (~2900 $cm^{-1}$ triplet and 1260 $cm^{-1}$ peak) did not exhibit this behavior, and they are identified with spectral artifacts. The 2900 $cm^{-1}$ triplet was also observed after a 1400 °C anneal that should remove all functional groups. All other IR peaks in the difference spectra of Figures 3 and 4 showed the anticipated increase in optical density with an increase in the SWNT film thickness on the substrate.

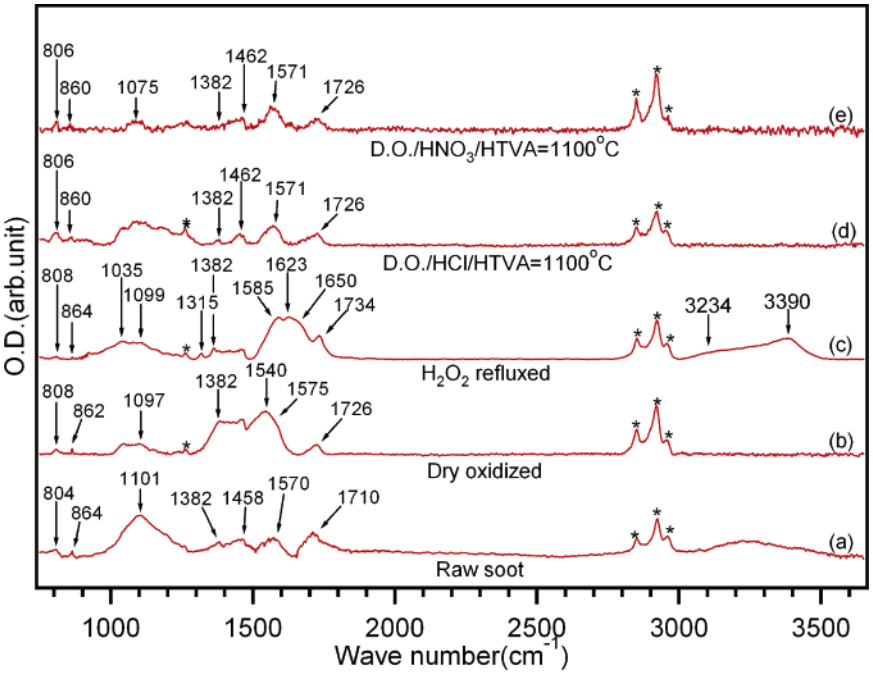


***Figure 3.*** Difference spectra from subtracting the polynomial background from the raw data (see caption to Figure 2) for raw SWNT soot (a), DO (b), $H_2O_2$ (c), DO/HCl/HTVA at 1100 °C (d), and DO/$HNO_3$/HTVA at 1100 °C (e) SWNT processed material. The top two spectra on purified and annealed SWNTs represent the cleanest material. Bands identified with spectral artifacts are indicated with asterisks.[31]

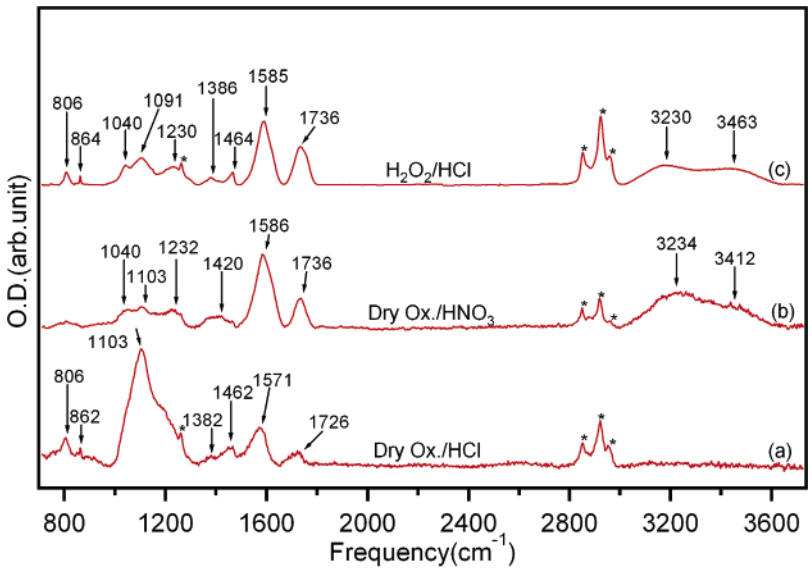


***Figure 4.*** Difference spectra from subtracting the polynomial background from the raw data (cf. caption to Figure 2) of chemically processed SWNT materials: DO/HCl (a), DO/$HNO_3$ (b), and $H_2O_2$/HCl (c). Spectral artifacts are indicated with asterisks.[31]

example, the 1101 $cm^{-1}$ band in Figure 3a is located within the range expected for C−O stretching modes in ethers, esters, alcohols, or phenol compounds, and the 1710 $cm^{-1}$ band can be assigned to carbonyl (C═O) stretching in ketones, aldehydes, or carboxylic acid groups.[30] For aldehyde groups, one or two bands assigned to the aldehydic C−H stretching, or the Fermi resonance between the fundamental aldehydic C−H stretching and the first overtone of the aldehydic C−H bending vibration, should generally appear in the 2695−2830 $cm^{-1}$ range.[32] However, these high-frequency bands are not observed, so the 1710 $cm^{-1}$ band is probably associated with either ketone or carboxylic acid groups. A prominent broad band (3100−3600 $cm^{-1}$) can be observed in two of the IR spectra of Figure 3. This broad band is assigned to contributions from a variety of O−H stretching modes. The width indicates that several different −OH containing groups are probably present in many different chemical and carbon environments. The frequency is somewhat lower than observed for free molecules and is instead characteristic of coupled acid and alcoholic hydroxyl functionalities. Since the −OH stretch band is present between 3100 and 3600 $cm^{-1}$, the C═O band at 1710 $cm^{-1}$ should probably be identified with carboxylic acid groups. We also should consider the presence of ketone groups. If a high frequency shoulder is seen on the ∼1710 $cm^{-1}$ band (the shoulder is apparent in the figure), we should also consider the presence of $\alpha,\beta$-unsaturated and benzoate esters. Since there is AC and possible polyaromatic hydrocarbons in the raw soot, it must be said that the functional groups we can see by their IR signature in the raw soot are not

necessarily on the tube walls but could be elsewhere in the sample. As reported by Zhang et al.,[16] a very broad band at ~1100 $cm^{-1}$ was observed in the raw SWNT soot grown by the CVD process. However, they did not make any assignment for this band. Zhang et al.[16] and Kukovecz et al.[12] did not observe a band at ~1700 $cm^{-1}$ in their raw soot samples.

After dry oxidation (DO) of the raw SWNT soot at 355 °C for 20 min (Figure 3(b)), the IR band at ~1100 $cm^{-1}$ is reduced, and the broad −OH absorption between 3100 and 3600 $cm^{-1}$ has been removed. These observations suggest that many of the functional groups seen in the spectrum of the raw soot (Figure 3a) may be attached to amorphous carbon or other carbonaceous fragments that were removed by dry oxidation. One intriguing feature in Figure 3b is the appearance of additional absorption in a broad band with structure located between ~1300 and 1600 $cm^{-1}$; we are unable to assign this band. It is also interesting that although very little or no change was observed in the Raman spectrum upon dry oxidation of the raw soot, a considerable change in the IR spectrum is evident. Our IR data show clearly that oxygen containing functional groups appear after dry oxidation (~1300 and 1600 $cm^{-1}$). Thus, IR can be seen to be a complimentary and powerful probe of chemical changes in this carbon system.

A reflux in 30% $H_2O_2$ has also been reported to remove AC from SWNT material.[6] The AC phase can be preferentially oxidized to $CO_2$ gas. For our $H_2O_2$-processed sample, the IR spectrum (Figure 3c) exhibits enhanced absorption near ~1730 $cm^{-1}$. This is consistent with the formation of additional carboxyl groups on the SWNT surface. The band in the $H_2O_2$ processed material is enhanced and upshifted to 1734 $cm^{-1}$, relative to its counterpart in the raw soot (~1710 $cm^{-1}$). After $H_2O_2$ reflux, very broad bands also appear in the ~3230−3500 $cm^{-1}$ range and are identified with O−H stretching modes. The broad low-frequency component of this O−H band with a peak at ~3234 $cm^{-1}$ (lower in intensity) is identified with O−H stretching from coupled carboxylic acid groups and the higher frequency band at ~3390 $cm^{-1}$ with alcoholic or phenolic groups. The frequency of these vibrations is sensitive to hydrogen bonding between functional groups. The low frequencies observed for both broad −OH bands in Figure 3b may be the result of coupling to adjacent oxygen containing groups. The C−O stretching vibrations in alcohols and phenols also exhibit bands in the 1000−1260 $cm^{-1}$ range; their frequency depends on the details of the coupling to C−C stretching vibrations. The bands at ~1035 and 1100 $cm^{-1}$, shown in the spectrum of Figure 3c, could therefore be tentatively identified with C−C−O stretching in unsaturated hydroxyl groups, and the small peak appearing at ~1315 $cm^{-1}$ in Figure 3c might be associated with the characteristic vibrational mode resulting from interaction between O−H bending and C−O stretching in phenol groups.[32]

There are several interesting changes in the IR spectrum at high frequency (>1500 $cm^{-1}$) after $H_2O_2$ processing. We observe a broadening and intensity enhancement of the absorption band in the 1550−1650 $cm^{-1}$ region. A band at ~1570 $cm^{-1}$ in the raw soot (Figure 3a) that we have identified with a fundamental SWNT mode[29] appears to have broadened and upshifted to ~1585 $cm^{-1}$ after $H_2O_2$ processing. It also now contains new structure at ~1620 and 1650 $cm^{-1}$, and the higher frequency modes are likely due to conjugation of C═O with C═C bonds or interaction between localized C═C bonds and carboxylic acids and ketones. Of course, there are many ways to couple and shift these high-frequency modes, so it is difficult to make definite assignments. For example, both intermolecular and intramolecular hydrogen bonding with hydroxyl groups result in delocalization of the $\pi$ electrons of both unsaturated groups or C═O groups. These couplings reduce the double-bond character of the C═O bond and downshift the IR bands. For example, the C═O stretching mode of a quinone group, without conjugation, usually appears at ~1715 $cm^{-1}$. Quinones that have both carbonyl groups in the same ring (which therefore has conjugation) absorb in the 1655−1690 $cm^{-1}$ region. With extended conjugation, in which the carbonyl groups are coupled weakly and appear in different rings, the absorption downshifts to the 1635−1655 $cm^{-1}$ region. Hence, there are many possibilities here, and model compound reactions with clean SWNT material will be needed to sort this out. Mawhinney et al. reported FTIR spectroscopic studies of the oxidation and etching of SWNTs using ozone at 298 K. They assigned a 1650 $cm^{-1}$ band to the C═O stretching mode of quinone groups added preferentially to the ends of the tubes.[18] In our case, the appearance of also O−H stretching modes after $H_2O_2$ reflux leads us to believe that coupling effects (i.e., both intermolecular and intramolecular hydrogen bonding with hydroxyl groups) also might be responsible for the downshift in the C═O stretching mode, besides the production of surface-bound quinone groups with extended conjugation.

It seems conclusive from an IR band analysis that an $H_2O_2$ reflux approach to AC removal leads to a substantial increase in carboxylic acid and hydroxyl (phenolic and alcoholic) groups relative to the amount found in the raw soot or after DO. At the same time, our Raman spectral analysis, discussed previously, shows an enhancement in the D-band scattering intensity and a broadening of the G-band for $H_2O_2$ processing but not for DO processing. From TGA and HRTEM, we know that $H_2O_2$ reflux definitely removes most of the AC component from the material. So, there is a consistent picture of the difference in the outcomes from dry oxidation (DO) and $H_2O_2$ reflux of raw SWNT material: while both oxidative processes lead to removal of AC, $H_2O_2$ reflux yields a much stronger functionalization of the nanotube wall. For electronic applications of processed SWNTs, for example, DO should be preferred. Recall that the $H_2O_2$ reflux was observed to upshift the G-band by ~ 4 $cm^{-1}$. The IR band that we have identified with one of the nanotube (tangential) IR modes also upshifts (by ~15 $cm^{-1}$). It can be seen from our work here that band upshifting can occur both by charge transfer ($NO_3^-$) and functionalization with negatively charged groups (−OH). In both cases, the upshifting of these tangential SWNT bands is associated with the withdrawal of $\pi$ electrons.

A SWNT is a macroscopic realization of a resonant C═C conjugated system. During strong chemical processing, it appears possible to create additional defects where carbon atoms are eliminated, the ring structure is now open, localized C═C bonds are created, and oxygen containing groups can be added to this defect to stabilize the structure. This should lead to an upshifting of the IR C═C bands, and a C═O band should appear. A strong coupling between neighboring C═O functional

(32) Silverstein, R. M.; Webster, F. X. *Spectrometric Identification of Organic Compounds*, John Wiley & Sons: New York, 1988; Ch. 3.

groups will downshift the C═O band and may be a signature of a high density of C═O groups. Zhang et al.[16] observed that the band at ~1735 $cm^{-1}$ that we identify with −COOH addition gradually downshifted to ~1720 $cm^{-1}$ with longer acid treatment. They suggested that longer acid treatment introduces more −COOH and −OH groups to the tube walls and ends, and this lowers the frequency of the −C═O stretching mode.[16] Their observation supports our assignment of new structures at ~1620 and 1650 $cm^{-1}$ that appear after refluxing the tubes in $H_2O_2$.

We next turn to the analysis of the IR spectroscopic signatures of acid processing of SWNT material to remove the metal growth catalyst. The material was first processed to remove the AC. In Figure 4, we show the IR spectra of DO/HCl (spectrum a) and DO/$HNO_3$ (spectrum b) processed material. The effects on the IR spectrum from $H_2O_2$/HCl processing are indicated in Figure 4c. We consider first the effect of HCl reflux on DO material. Basically, the only significant changes in the IR spectrum after HCl reflux is a reduction in the absorption near ~1400 $cm^{-1}$ and an enhancement in absorption near ~1100 $cm^{-1}$. As discussed previously, we have had difficulty assigning the 1400 $cm^{-1}$ band to a particular functionality. The fact that the 1400 $cm^{-1}$ band intensity is reduced certainly strengthens our opinion that the ~1400 $cm^{-1}$ band is associated with an unknown functional group rather than a nanotube mode. Earlier, we assigned the ~1100 $cm^{-1}$ band to C−O stretching; C−O containing groups appear to have been added by HCl reflux. However, the chemistry behind these C−O additions needs to be clarified in further work.

Interestingly, for DO/HCl processing of raw SWNT soot, little or no changes in the Raman scattering from the D- or the G-bands were observed (i.e., the D-band intensity and the G-band component widths did not change). However, the IR spectrum shows a clear change: C−O containing functional groups have been added to the tube wall. Hence, the reduction in the Raman intensity $I_R/I_G$ for DO/HCl processed SWNT must be due to C−O functionalization.

Processing DO material with $HNO_3$ can be seen in Figure 4b to lead to the addition of carboxylic acid and hydroxyl groups (cf., broad bands with maxima at ~3234 and ~3412 $cm^{-1}$). From the relative intensity of these two broad components, we can conclude that $HNO_3$ leads to a larger population of carboxyl relative to hydroxyl group on the SWNT wall. Several groups[12,16,17] have also observed the enhancement of the band at ~1730 $cm^{-1}$ after refluxing SWNT samples in $HNO_3$ or a mixed acid such as $HNO_3/H_2SO_4$. They assigned this band to a C═O stretching mode in carboxylic acid groups. We also observe an upshift in the SWNT band at ~1575 $cm^{-1}$ (DO) to ~1586 $cm^{-1}$ (DO/$HNO_3$) that is consistent with charge transfer (i.e., via the attachment of $NO_3^-$ ions) and possibly mitigated by localization of C═C bonds and coupling to C═O modes, as discussed previously. The band in the DO/$HNO_3$ material (Figure 4b) at ~1230 $cm^{-1}$ probably should be assigned to the O−H bending mode or C−O stretching mode.

We next consider, from the perspective of IR spectroscopy, the effect of a completely wet purification of the SWNT soot (i.e., $H_2O_2$ reflux to remove the amorphous carbon and a mild mineral acid reflux (HCl) to remove the metal). To see the effects of HCl on the wet oxidized material, we need to compare spectrum c in Figure 4 to that discussed previously in Figure 3. From this comparison, it is clear that HCl induces replacement reactions that remove many of the oxygen containing functional groups. This view is consistent with two observations: (i) the broad ~3390 $cm^{-1}$ O−H stretching band in $H_2O_2$ refluxed material (Figure 3c) (from the hydroxyl groups) is now less intense. The high-frequency component is also upshifted from 3390 to 3460 $cm^{-1}$, indicating a decoupling of hydroxyl groups, consistent with a decrease in their population. (ii) The broad strong bands in the ~1500−1700 $cm^{-1}$ region for $H_2O_2$ refluxed material (Figure 3c) show a significant reduction in intensity. The bands are now narrower. Similar to the IR spectrum for the DO/$HNO_3$ material, one relatively sharp band at ~1585 $cm^{-1}$ identified with the IR active tangential nanotube mode is observed, upshifted by charge transfer from its position at ~1570 $cm^{-1}$ in the raw soot.

Finally, we consider the IR signatures that evolve from a short term high-temperature vacuum anneal (HTVA) of the DO/HCl and DO/$HNO_3$ material. These spectra appear at the top of Figure 3. We have discussed the outcome from this anneal from the perspective of the Raman bands. As discussed previously, the Raman data show that an anneal in ~1100 °C in a vacuum for 1 h reduces the D-band intensity and the G-band component width, returning the SWNT structure to almost the same condition as was observed for tubes in the raw soot. We expect that high temperatures should remove many of the functional groups produced by dry or wet chemical processing. Indeed, according to a review of many studies of functional groups on high surface area amorphous and graphitic carbons by Kinoshita,[30a] various groups leave at characteristic temperatures. Summarizing his review, carboxylic and lactone groups begin to decompose first at about 250 °C and are volatilized. In the 500−900 °C range, phenol and quinone groups have decomposed almost entirely. And at 900 °C, the −OH content decreases significantly, and other oxygen containing surface groups are almost completely eliminated. Hydrogen, on the other hand, is removed from amorphous carbon by heat treatment between 900 and 1200 °C. On the basis of the review by Kinoshita,[30a] our HTVA at 1100 °C for 1 h should remove all oxygen containing functional groups; we expect also that any −CH groups present should also be decreased drastically.[29]

Comparing the IR spectra for DO/$HNO_3$/HTVA and DO/HCl/HTVA to that of the raw soot (cf., Figure 3a,d,e), we see that the broad bands in the 3000−3600 $cm^{-1}$ region are removed, as well as many of the broader and stronger bands below 1600 $cm^{-1}$ present in the starting material. Furthermore, after removal of AC by $H_2O_2$ reflux (cf., Figure 3c) and DO (cf., Figure 3b), broad −OH bands remain in the material, which we have attributed to functional groups. By comparing the top two IR spectra in Figure 3 to those that appear below in the same figure, as well as to those for acid-processed material in Figure 4, we can say that HTVA indeed removes most of the functional groups either present in the starting material or added by chemical processing.

However, it is clear from the top two IR spectra in Figure 3 that there are some small differences in the purified HTVA material, depending on whether HCl or $HNO_3$ was used to remove the metal. Annealing of the DO/HCl material at higher temperatures (up to ~1400 °C) generated a material whose IR spectrum is almost identical to that shown for DO/$HNO_3$/HTVA material in Figure 3e. The weak structure that remains in spectra d and e of Figure 3 for HTVA purified SWNT material below

***Table 1.*** IR Bands Observed in the Raw and Chemically Processed SWNT Material[a]

| observed band | chemical processing | assignment |
|---|---|---|
| ~1100 $cm^{-1}$ | raw soot, DO, $H_2O_2$, DO/HCl, DO/$HNO_3$, $H_2O_2$/HCl | C−O stretching in ethers, esters, alcohol, and phenol compounds |
| ~1230 $cm^{-1}$ | DO/$HNO_3$, $H_2O_2$/HCl | O−H bending or C−O stretching |
| ~1315 $cm^{-1}$ | $H_2O_2$ | interaction between O−H bending and C−O stretching in phenol groups |
| ~1500 to ~1660 $cm^{-1}$ | $H_2O_2$, DO/$HNO_3$, $H_2O_2$/HCl | conjugation of C═O with C═C bonds or interaction between localized C═C bonds and carboxylic acids and ketones |
| ~1710 to ~1734 $cm^{-1}$ | raw soot, DO, $H_2O_2$, DO/HCl, DO/$HNO_3$, $H_2O_2$/HCl | C═O stretching in ketone or carboxylic acid groups |
| ~ 3230 $cm^{-1}$ | raw soot, $H_2O_2$,DO/$HNO_3$, $H_2O_2$/HCl | O−H stretching in coupled carboxylic acid groups |
| ~3400 $cm^{-1}$ | raw soot, $H_2O_2$, DO/$HNO_3$, $H_2O_2$/HCl | O−H stretching in alcoholic or phenolic groups |

[a] The second column indicates the processing applied before the spectra were observed.

~1700 $cm^{-1}$ has been discussed in terms of the predicted one- and two-phonon IR absorption by Kim et al.[29] The band positions for the weak structure that remain after HTVA are reported to be in reasonable agreement with theory.[29]

In Table 1, we summarize the main IR bands observed for functional groups in the raw soot and chemical processed SWNT material, as well as our assignment for those bands. The assignments we make in Table 1 are plausible but are by no means certain. Follow-on work on model compounds will need to be done to confirm these tentative assignments.

In summary, this work presents a first step toward the use of IR and Raman spectroscopy as a probe for SWNT chemistry and the evaluation of purified SWNT material after reactions. We expect that much progress will now be made in understanding SWNT chemistry, as cleaner SWNT material becomes available and these spectroscopies are applied to probe the material. Higher annealing temperatures should be avoided, however, as nanotube coalescence and other transformations begin to take place at 1400−1600 °C.[22] This work represents an early study using both IR and Raman spectroscopy to observe the effect of several common chemical schemes to remove amorphous carbon and growth catalysts from large batches of ARC derived SWNTs. Our objective was to learn which of these processes produced the most damage to the carbon skeleton and which functionalities were added via exposure to specific chemicals. This work is one of the first, if not the first, to indicate which purification procedure is to be preferred based on observations of damage to the carbon skeleton or added functionalities. This work is the first of its kind to address purification from the vantage point of vibrational spectroscopy. Considerable progress, however, is needed to take this work to a higher (more quantitative) level, such as could be obtained from correlating IR intensities with percent functionalization. This type of study is best done with model SWNT compounds. In the present work, we must be content to simply learn about the effects of the particular (commonly used) purification scheme by noticing how they affect the D-band Raman scattering, or for example, when the intensity from carboxyl vibrations increases or decreases. The next step, set aside for future work, is to make quantitative contact between IR spectroscopy (e.g., IR band intensities) and some other probe (e.g., TG-MS) that can tell us about the nature and quantity of functionalites present. It is hoped that this work will spark interest in model compound reactions of SWNTs with various reagents and that IR and Raman spectroscopy can be used to characterize the reactions.

**Acknowledgment.** The authors thank Dr. B. Pradhan, Columbia Chemical, Inc., for many helpful discussions on this topic and for his initial work with us in this area. We also thank A. Gupta for help in taking some of the early IR spectra in this study. We also thank M. S. C. Mazzoni, UFMG, Department of Physics, Brazil for the SWNT figures. C.A.F. thanks the Brazilian funding agency $CNP_q$ for supporting her visit to Penn State University where much of this work was carried out. The work at Penn State was carried out, in part, by support from the NSF-NIRT (NSF-DMR-0103585 and NSF-DMR-0304178).

JA052951O